Petroleum Science 20 (2023) 1087–1103

Contents lists available at ScienceDirect

Petroleum Science

journal homepage: www.keaipublishing.com/en/journals/petroleum-science

Original Paper

Performances of a Stinger PDC cutter breaking granite: Cutting force and mechanical specific energy in single cutter tests

Chao Xiong [a], Zhong-Wei Huang [a, *], Huai-Zhong Shi [a], Rui-Yue Yang [a], Gang Wu [b], Han Chen [a], Wen-Hao He [a]

[a] China University of Petroleum (Beijing), Beijing, 102249, China
[b] Dagang Oilfield Company, Tianjin Gas Storage Branch, Tianjin, 300280, China

ARTICLE INFO

Article history:
Received 18 April 2022
Received in revised form
10 October 2022
Accepted 12 October 2022
Available online 17 October 2022

Edited by Yan-Hua Sun

Keywords:
Stinger PDC cutter
Cutting force
Mechanical specific energy
Single cutter tests

ABSTRACT

The Stinger PDC cutter has high rock-breaking efficiency and excellent impact and wear resistance, which can significantly increase the rate of penetration (ROP) and extend PDC bit life for drilling hard and abrasive formation. The knowledge of force response and mechanical specific energy (MSE) for the Stinger PDC cutter is of great importance for improving the cutter's performance and optimizing the hybrid PDC bit design. In this paper, 87 single cutter tests were conducted on the granite. A new method for precisely obtaining the rock broken volume was proposed. The influences of cutting depth, cutting angle, and cutting speed on cutting force and MSE were analyzed. Besides, a phenomenological cutting force model of the Stinger PDC cutter was established by regression of experimental data. Moreover, the surface topography and fracture morphology of the cutting groove and large size cuttings were measured by a 3D profilometer and a scanning electron microscope (SEM). Finally, the rock-breaking mechanism of the Stinger PDC cutter was illustrated. The results indicated that the cutting depth has the greatest influence on the cutting force and MSE, while the cutting speed has no obvious effects, especially at low cutting speeds. As the increase of cutting depth, the cutting force increases linearly, and MSE reduces with a quadratic polynomial relationship. When the cutting angle raises from 10° to 30°, the cutting force increases linearly, and the MSE firstly decreases and then increases. The optimal cutting angle for breaking rock is approximately 20°. The Stinger PDC cutter breaks granite mainly by high concentrated point loading and tensile failure, which can observably improve the rock breaking efficiency. The key findings of this work will help to reveal the rock-breaking mechanisms and optimize the cutter arrangement for the Stinger PDC cutter.

1. Introduction

Since the polycrystalline diamond compact (PDC) cutter was invented in the 1970s, PDC bits have been commonly employed in oil & gas drilling and geothermal drilling due to the high rock breaking efficiency and long duration life (Dai et al., 2021a; Zhu et al., 2022). However, in deep/ultra-deep hard rock formations, conventional PDC cutters still faced severe wear and impact failure challenges (Jamali et al., 2019). In 2010, a conical-shaped PDC cutter (Stinger PDC cutter) was invented, which has twice the thickness of the polycrystalline diamond layer as conventional PDC cutters, and the wear and impact resistance are improved by 25% and 100% respectively as shown in Fig. 1 (Azar et al., 2013). During the last ten years, the hybrid PDC bit, on which the Stinger PDC cutter is strategically positioned at the bit center or behind the conventional PDC cutter, has completed more than 33 million feet of drilling, and the drill bit footage and rate of penetration (ROP) were significantly improved in hard and interbed formation (Gunawan et al., 2018; Schlumberger, 2022).

Although the hybrid PDC bit has been widely used in the drilling fields (Al-Enezi et al., 2017; German et al., 2015; Gunawan et al., 2018), the study of Stinger PDC cutters breaking hard rock is relatively few. The fundamental research is lagging behind the field application of hybrid PDC bits. The excellent rock-breaking performance of Stinger PDC cutters has not yet been brought into play. The single cutter test is considered an effective and straightforward way to research the cutting performance and mechanism of PDC cutters (Cheng et al., 2019a; Zijsling, 1987). Hence, former

* Corresponding author.
E-mail address: huangzw@cup.edu.cn (Z.-W. Huang).

https://doi.org/10.1016/j.petsci.2022.10.006

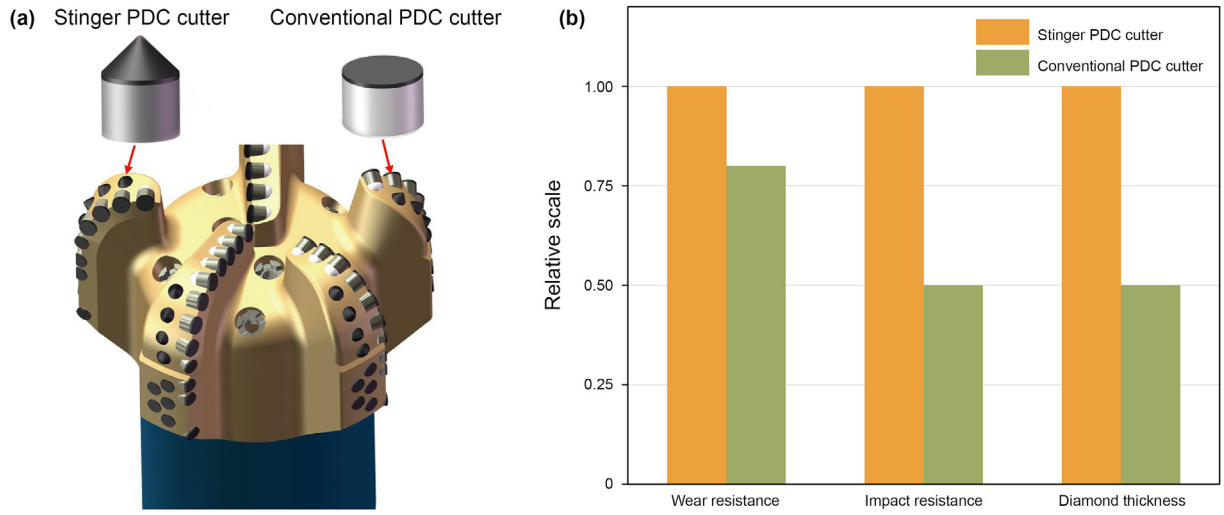

Fig. 1. (**a**) The shape of conventional and Stinger PDC cutters and their location on the hybrid PDC bit; **(b)** Comparison of two cutters' performances (Azar et al., 2013).

researchers have conducted a large number of single cutter tests to investigate the force responses, cutting efficiency, chip formation, and rock failure behavior during the cutting process of conventional PDC cutters (Aresh et al., 2022; Che et al., 2017; Cheng et al., 2018; Dai et al., 2021a; Rajabov et al., 2012). For the Stinger PDC cutter, Durrand et al. (2010) tested the impact resistance, wear resistance, and life duration in the laboratory for the first time. Since then, many researchers studied the rock-breaking characteristics of Stinger PDC cutters. Sun et al. (2014) conducted single cutter tests to research the variations of cutting force with cone tip diameter, cutting angle, and rock hardness. He (2014) and Dou and Yang (2015) established a numerical model to study the influence of cutting angle, cone tip angle, cone tip diameter and cutting depth on the rock breaking efficiency. Hempton et al. (2015) carried out the impact experiments with a single PDC cutter. The results showed that under the condition of 80 kN impact force, conventional PDC cutters are broken after one impact, but Stinger PDC cutters are still not damaged after 100 impacts. Liu et al. (2019) studied the cutting force and rock-breaking efficiency under different pre-cutting depths when the Stinger and conventional PDC cutter are placed at the same track. Xiong et al. (2020b) carried out single cutter tests with Stinger and conventional PDC cutters respectively. The difference in cutting characteristics and rock-breaking mechanism between the two kinds of cutters were analyzed. Compared with conventional PDC cutters, Stinger PDC cutters have 46.14% less cutting force and 34.09% higher rock-breaking efficiency. In addition, Xiong et al. (2021) established a 3D cutting force analytical model considering the influences of confining pressure and thermal stress. Xiong et al. (2022) carried out mixed tool cutting granite experiments with Stinger and conventional PDC cutters. The influences of the cutting sequence, spacing, and depth difference of mixed cutters on the effect of rock breaking were analyzed.

The above studies are mainly focused on the test of characteristics of the Stinger PDC cutter. There is a lack of systematic and in-depth experimental research on the mechanism of Stinger PDC cutters breaking hard rock. Furthermore, the cutting force and mechanical specific energy (MSE) of a single cutter directly determine the whole PDC bits' working stability and drilling efficiency (Chen et al., 2021; Glowka, 1989). Investigating the cutting performance and mechanism of a single Stinger PDC cutter can provide theoretical guidance for the hybrid PDC bit design and further improve the ROP. In this paper, a single cutter test experimental setup was developed and a series of cutting tests were conducted on the granite by a Stinger PDC cutter. A new method of precise obtaining the rock broken volume is proposed: the *x*, *y*, and *z* coordinates of each point on the surface of the cutting groove were measured by the ST400 3D Profilometer. Then, the shape of the cutting groove was rebuilt and the rock broken volume was calculated. Furthermore, the influences of cutting depth, cutting angle, and cutting speed on cutting force and MSE were analyzed and discussed, and a phenomenological cutting force model is established based on the experimental data. Finally, the surface topography and fracture morphology of the cutting grove and large-size cuttings are discussed to reveal the rock-breaking mechanism of Stinger PDC cutters.

2. Experimental

2.1. Experimental setup

An experimental apparatus was developed for single cutter tests as shown in Fig. 2. It mainly consists of a cutter and rock sample clamping system, a movement system, and a control/measurement system. The rock sample is fixed on the horizontal bed with two long bolts and a flat plate. The horizontal bed driven by an electric motor can move on the two horizontal guide rails with a constant velocity (1.6–230 mm/s). The Stinger PDC cutter is mounted on the clamps and locked by three locking screws once the cutting depth and cutting angle are set well. During the cutting process, the Stinger PDC cutter stayed still, and the rock moves in a straight line. Four load sensors are mounted in front of the rock sample along the cutting direction to measure the cutting force. The range and accuracy of the sensors are 0–10 kN and 1 N, respectively, which can meet the cutting force measurement in the experiment of single PDC cutter breaking rock (Che and Ehmann, 2014). The control/measurement system can control the cutting speed/cutting length and records the cutting force. More details of this experimental apparatus were introduced in our previous work (Dai et al., 2021b).

2.2. Cutters and rock materials

In this research, the oilfield commonly used Stinger PDC cutter was selected to carry out cutting experiments. This cutter was produced by Wuhan Ninestones Superabrasives Co., Ltd, which consists of a diamond layer and a tungsten carbide (WC) stud. The

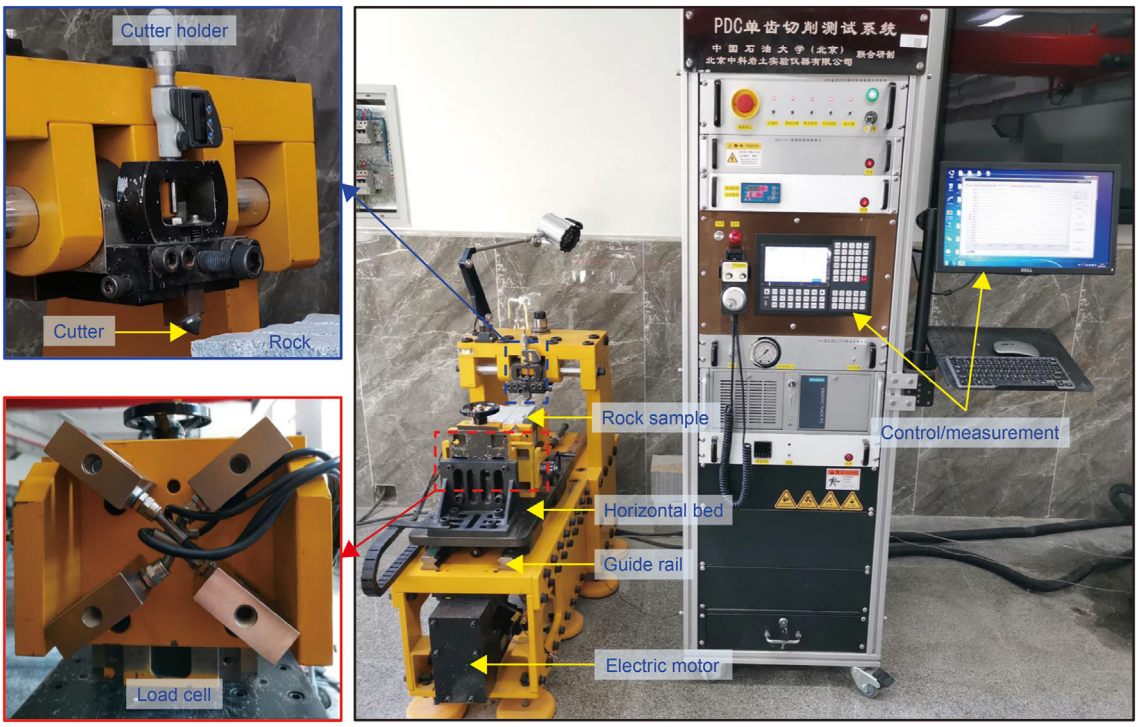

Fig. 2. Experimental setup for the single cutter tests.

geometric parameters were shown in Fig. 3(a). Before the experiment, the Stinger PDC cutter is mounted on the cutter clamp with super glue as shown in Fig. 3(b). The cutter clamp is designed with different inclination angles, e.g., 0°, 10°, 20°, 30°, etc. In addition, the inclination angle can also be fine-tuned within the range of 0°–10° by rotating the cutter holder. The resolution of the angle fine tuning is 1°. Therefore, the cutting angle can be adjusted by selecting an appropriate cutter clamp and rotating the cutter holder to satisfy the requirements of experiments.

As shown in Fig. 3(c), the granite rock sample used in single cutter tests was collected from outcrops in Shandong Province, China. The mineral compositions are measured by X-ray diffraction (XRD) as shown in Table 1, it mainly consists of K-feldspar (38.3%), and plagioclase (29.9%). Moreover, the physical and mechanical properties of this granite are also tested by RTR-1500 HTHP rock triaxial apparatus. The main parameters of the system are as follows: a maximum loading confining pressure of 140 MPa, a maximum axial static pressure of 1000 kN, a maximum axial dynamic pressure of 800 kN, and a maximum sample diameter of 54 mm. The basic physical and mechanical properties of granite are shown in Table 2. Before the cutting experiment, the large size granite blocks with no obvious cracks or other damages were selected and cut into small cube blocks with 150 × 150 × 150 mm^3.

2.3. Experimental procedures

In this study, 29 experimental scenarios were designed under different cutting parameters including the depth of cut (DOC), the cutting angle (γ), and the cutting speed (v_c). In the drilling field, the bottom-hole rock is removed layer by layer. The thickness of a layer corresponds to the cutting depth of PDC cutters for the laboratory cutting experiment. According to the drilling speed and rotary speed data of PDC bits used in the northwest Chocolate Mountains geothermal drilling projects (Raymond et al., 2012), it can be calculated that the thickness of each layer is between 1 and 3 mm. Thus, in this experiment, the cutting depth is set to five levels, i.e.:1.0, 1.5, 2.0, 2.5, and 3.0 mm. During the hybrid PDC bits design, the rake angle of Stinger PDC cutters is generally less than 30°. In

Fig. 3. The Stinger PDC cutter and granite sample used in the tests: **(a)** Stinger PDC cutter parameters; **(b)** Cutter clamps with different inclination angles; **(c)** Granite block.

Table 1
Mineral compositions of granite specimens tested by XRD.

Mineral composition	Quartz	K-feldspar	Plagioclase	Dolomite	Siderite	Pyrite	Amphibole	Glauberite	Augite	Clay minerals
Content, %	9.7	38.3	29.9	2.4	0.5	0.4	8.3	3.6	6.3	0.6

Table 2
Basic physical and mechanical properties of granite specimens.

Properties	Density, g/cm^3	Young's modulus, GPa	Poison's ratio	Cohesive strength, MPa	Internal friction angle, degree	Tensile strength, MPa	UCS, MPa
Avg	2.63	41.30	0.27	42.29	46.19	11.16	129.78
SD	0.02	2.08	0.01	2.60	3.46	2.08	10.48

Note: The properties were tested three times; Avg represents the average value of the results for the tests and SD is the standard deviation.

previous studies, the cutting angle of Stinger PDC cutters in single cutter tests was usually chosen at 10°–30° (Sun et al., 2014). Thus, in this paper, the cutting angle is set to five levels, i.e.: 10°, 15°, 20°, 25°, and 30°. Referring to the cutting speed chosen by former researchers for conventional PDC cutters cutting rocks (Cheng et al., 2018), the cutting speed is set to five levels, i.e.: 5, 10, 15, 20, and 25 mm/s. Each experiment was conducted three times on the same surface of the granite sample to reduce the experimental error.

During the cutting process, the cutting depth should be kept constant. So, before the experiment, the rock surfaces were finished with high-precision machine tools to ensure parallelism and flatness. The experimental procedure is as follows: (1) put the prepared granite sample on the horizontal bed, and use the rock clamping system to fix the rock sample; (2) put the Stinger PDC cutter clamp on the cutter holder, adjust the cutting angle and the cutting depth, then lock the cutter clamp to ensure the Stinger PDC cutter could not move during the cutting process; (3) set the cutting speed and cutting distance (180 mm) on the control/measurement panel; (4) open data acquisition and control software, click the "Start" button on the control/measurement panel and the software interface. The horizontal bed and the rock sample are driven by the electric motor to move along the horizontal guide rail and the cutting experiment begins. The cutting force was recorded with a sample rate of 200 points/s during the whole cutting period; (5) after the cutting tests, open the rock clamping system, take out the granite sample, and one cutting test is finished.

2.4. Experimental data processing method

Fig. 4 shows a set of typical experimental data which is the cutting force variation with the cutting distance at different cutting depths. It is clearly shown that the cutting force has significant oscillations due to the brittle fracture characteristics and the inhomogeneous microstructure of the rock (Che et al., 2017; Dai et al., 2021a). The cutting force varies periodically and constantly repeats a process: gradually increasing, reaching a peak, and then decreasing rapidly. The average deviation of cutting force at 1, 1.5, 2.0, 2.5, and 3.0 mm cutting depth is 575, 854, 1067, 1148, and 1385 respectively, which can be used to evaluate the degree of data fluctuation (Dai et al., 2020). When the cutting depth increases, the fluctuation amplitude of the cutting force significantly increases. This is because the rock is broken with the brittle failure mode as the cutting depth is deep and at the shallow cutting depth, the rock is mainly broken with ductile failure mode (He and Xu, 2015; Liu et al., 2018). In addition, the average cutting force is considered as a good representative of the dynamic cutting force responses in single cutter tests (Che et al., 2017). In this paper, the cutting force at the cutting distance ranging from 40 to 160 mm is selected to calculate the average cutting force to decrease the error caused by the boundary effects (Xiong et al., 2020b). Except for special instructions, the cutting forces in this article are average cutting forces.

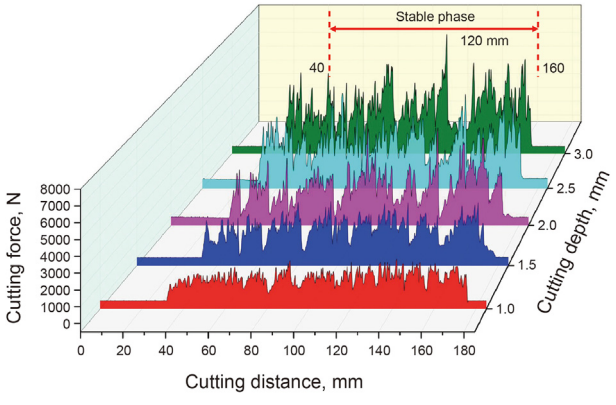

Fig. 4. The variation of cutting force with cutting distance ($v_c = 5$ mm/ s and $\gamma = 30°$).

Mechanical specific energy (MSE) is defined as the amount of mechanical energy consumed for breaking a unit volume of rock (Teale, 1965). In single cutter tests, the cutting depth is fixed, thus the work done by the normal force is zero. The MSE can be simplified as (Rafatian et al., 2010):

$$E_{ms} = \frac{Q}{V} = \frac{F_c \times L}{V} \tag{1}$$

where E_{ms} is the mechanical energy; Q is the work done by the cutter in the cutting process, J; V is the rock broken volume, m^3; F_c is the average cutting force, N; L is the cutting distance, m.

According to Eq. (1), accurately estimating the rock broken volume is crucially important for calculating MSE. For conventional PDC cutters, the cutting groove has regular geometric shapes as shown in Fig. 5(a). The cross-section is a regular arc, which is related to the diameter of cutters, cutting depths, and cutting angles. Thus, the rock broken volume can be easily calculated by the analytical method. However, due to the completely different cutter shapes and rock-breaking mechanism between the Stinger and conventional PDC cutters, the cutting groove geometric shape of Stinger PDC cutters is very irregular as shown in Fig. 5(b). Thus, it is very difficult to calculate the rock broken volume by cutting parameters and geometric parameters of Stinger PDC cutters.

In this paper, a new method is proposed to obtain the rock broken volume: first, the ST400 3D Profilometer, which is a noncontact device designed with leading-edge chromatic confocal technology, is used to scan the surface topography of cutting grooves; then, the x, y, and z coordinates of each point on the

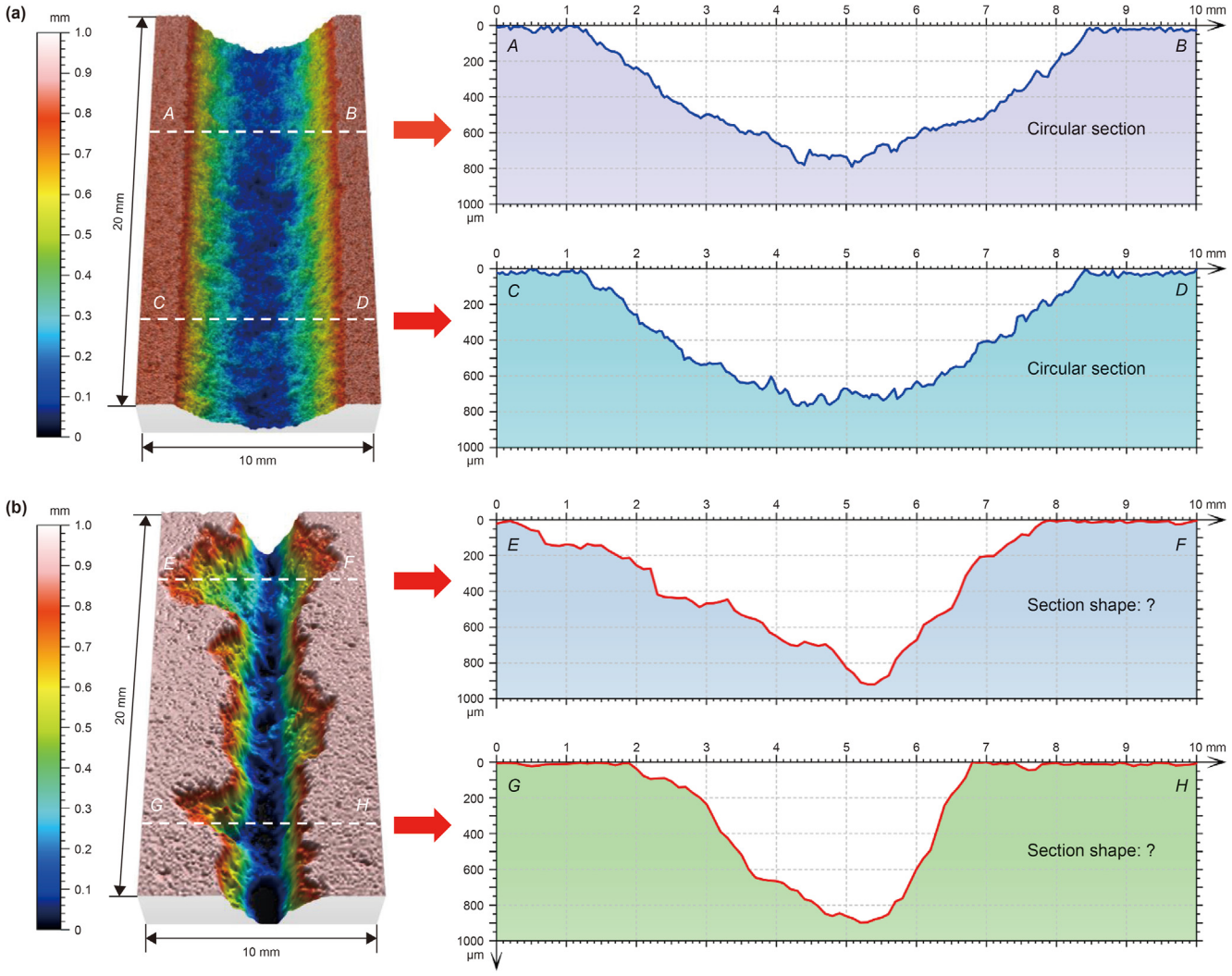

Fig. 5. The geometric shape of cutting grooves: **(a)** Regular shape formed by a conventional PDC cutter; **(b)** Irregular shape formed by a Stinger PDC cutter.

surfaces of the cutting groove are accurately measured and recorded; last, based on the coordinates of these points, the shape of cutting groove can be rebuilt and rock broken volume can be calculated by programming. As shown in Fig. 6, assuming the points *A*, *B*, *C*, and *D* are located on the surface of the cutting groove, the volume of micro-unit *ABCDEFGH* can be approximately expressed as:

$$V_i = \frac{1}{4}\Delta x \cdot \Delta y \cdot (z_1 + z_2 + z_3 + z_4) \tag{2}$$

thus, the rock broken volume can be calculated by adding the volumes of all the micro-units, which can be expressed as:

$$V = \sum_{i=1}^{n} V_i \tag{3}$$

After the single cutter tests, all cutting grooves were measured by the ST400 3D Profilometer. The scanned cutting groove length is 100 mm. The measurement resolution in the *x*-axis and the *y*-axis direction is set as 20 μm. In other words, Δ*x* and Δ*y* are 20 μm. Then, the rock broken volumes were calculated by the programming according to Eqs. (2) and (3). Last, MSE was calculated by Eq. (1).

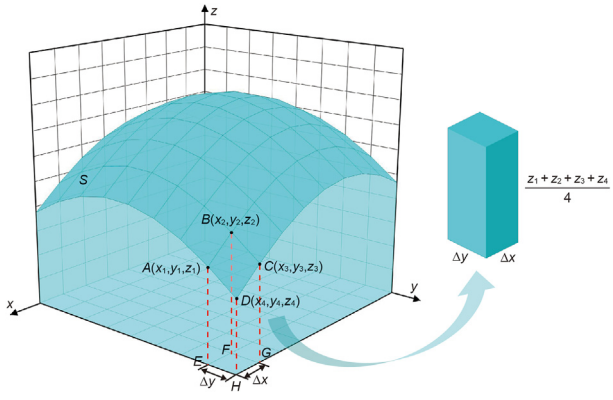

Fig. 6. The schematic diagram of calculating rock broken volume according to *x*, *y*, and *z* coordinates of each point on the cutting groove surface.

3. Experimental results

3.1. Influence of cutting parameters on cutting force

Studying the influence of cutting parameters on cutting force

can help to optimize the cutter arrangement design of hybrid PDC bits. Fig. 7 shows the variation of cutting force with the cutting depth. It can be noted that the cutting force has the same variation tendency at different cutting angles. When the cutting depth is shallow, the cutting force is small. With the rise of cutting depth, the cutting force gradually increases. By fitting analysis, there is a good linear function correlation between the cutting force and the cutting depth. For the conventional PDC cutter, it is generally accepted in the literature that the cutting force increases with the cutting depth (Che et al., 2017; Dai et al., 2020). It can be concluded that the variation trend of cutting force with cutting depth is independent of cutter geometry.

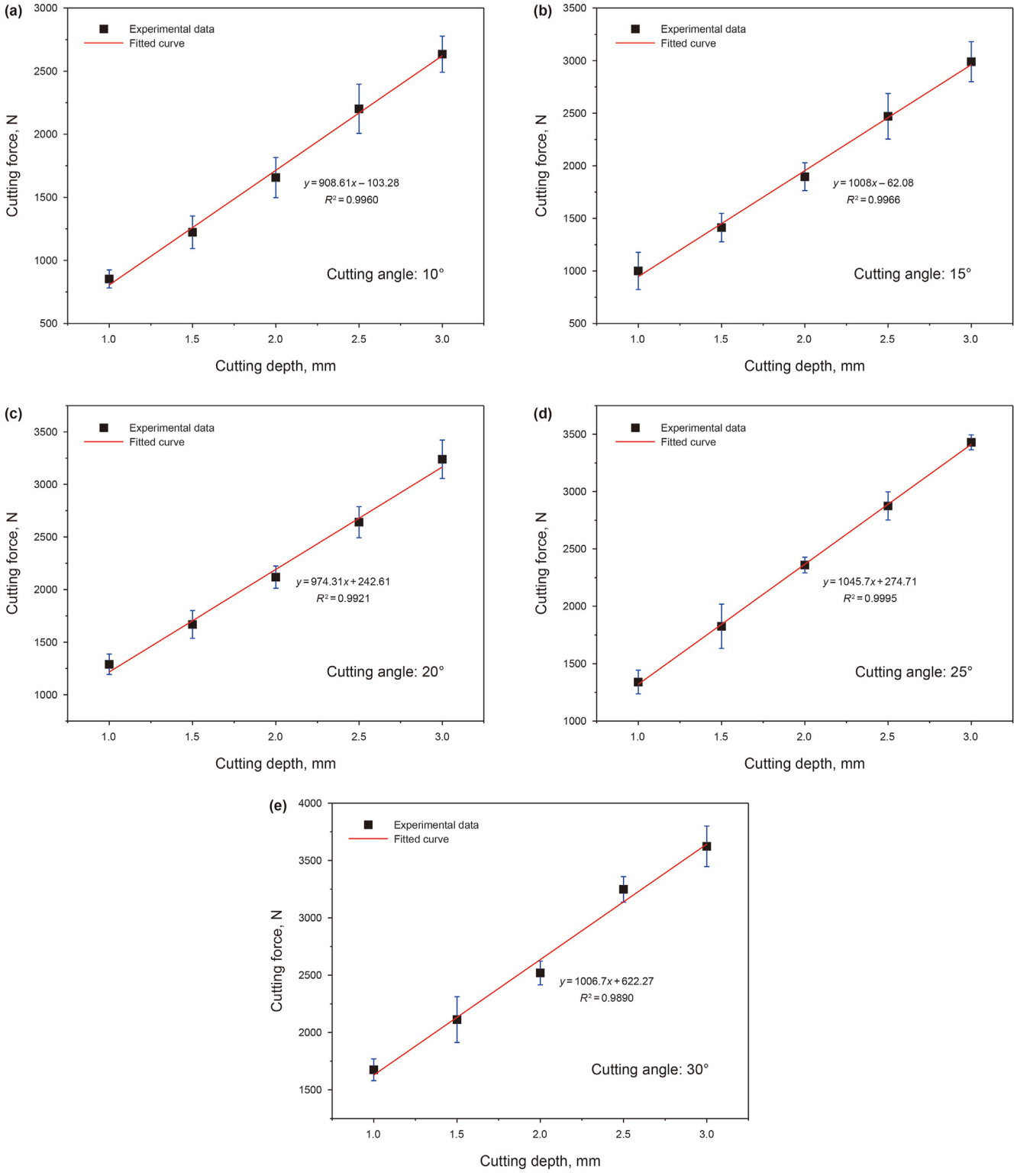

Fig. 7. The variation of cutting force with cutting depth at different cutting angles.

The cross-section area of cutting grooves has a great influence on the cutting force. The larger cross-section area means that more rock in front of the cutter needs to be removed, thus a larger cutting force needs to be applied. Cheatham Jr and Daniels (1979) quantitatively evaluated the relationship between cutting force and cross-section area based on the experimental data. They concluded that cutting force is proportional to the cross-section area. In addition, the cross-section area is predominantly affected by the cutting depth except for the geometry parameters of the PDC cutter. An increase in the cutting depth leads to an increase in cross-section area. For instance, the cross-section area of the cutting groove produced by the Stinger PDC cutter in this paper is approximately 1.0 and 9.0 mm^2 in theory when the cutting depth is 1 and 3 mm, respectively. The cross-section area for 3 mm cutting depth is remarkedly larger than that of 1 mm cutting depth. Therefore, the cutting force increases with increasing cutting depth at all cutting angles shown in Fig. 7.

Fig. 8 shows the variation of cutting force with the cutting angle at different cutting depths. As increasing the cutting angle, the cutting force increases linearly. Many researchers also concluded that the cutting force of a conventional PDC cutter increases with increasing the cutting angle (Coudyzer and Richard, 2005; Rajabov et al., 2012; Rostamsowlat et al., 2018). This variation trend of cutting force with cutting angle is consistent with that of the Stinger PDC cutter. The reasons for increased cutting forces of the Stinger PDC cutter with increasing back rake angle can be attributed to the fact that the cutter-rock interaction area increases with the rise of the cutting angle. The increased interaction area causes the cutter needs to overcome greater friction force, thus the larger cutting force needs to be applied for breaking the same rock. In this paper, at 3 mm cutting depth, the cutter-rock interaction area at a 10° cutting angle is 19.5 mm^2. At the 30° cutting angle, it is 38.9 mm^2 which enlarges 100% more than the 10° cutting angle.

As shown in Fig. 9, the cutting force is plotted at different cutting speeds. With the increase in cutting speed, the cutting force nearly keeps constant, which indicates that the cutting speed ranging from 5 to 25 mm/s has no obvious influence on the cutting force. Rock fragmentation is the process of micro-cracks generation and propagation under the forces of PDC cutters. The crack propagation speed is far greater than the cutting speed (Che et al., 2018). Thus, the impacts of cutting speed on the cutting processes can be nearly ignored.

3.2. A phenomenological cutting force model

During the PDC bit design, estimating the bit force response is an important job, which directly affects the working stability, drilling efficiency, and the duration life of PDC bits. However, a force response model of the PDC bit is usually derived by integrating the force contribution from all the cutters (Chen et al., 2021). To this end, numerous single cutter force models for the conventional PDC cutter were established. Cheatham Jr and Daniels (1979) firstly concluded that the cutting force is proportional to the cross-section area of the cutting groove based on their experimental results. Following this conclusion, many phenomenological force models for the conventional PDC cutters were developed, which can be classified as the cutting area-based model—namely, the cutting force is proportional to the cross-section area (Chen et al., 2016; Jianyong, 2012; Richard et al., 2010).

However, it should be noted that, for conventional PDC cutters, the interaction face between the cutter and rock is a plane. The Stinger PDC cutter is a three-dimensional cutter and the interaction face of the cutter-rock is a conical surface. In addition, the conventional PDC cutter has a sharp ledge that cuts the rock mainly with shearing action, while the Stinger PDC cutter break rock with plowing action (Xiong et al., 2020b). These differences can be reflected in the geometric shape of cutting grooves in Fig. 5. The Stinger PDC cutter has a completely different rock-breaking mode and force response than conventional PDC cutters. Fig. 10(a-1) and (b-1) present the schematic of force responses for the conventional and Stinger PDC cutter. From a physical perspective, N is generated by the squeezing effect of cutters and it's perpendicular to the cutter's rake face while S is generated due to the frictional action (Che et al., 2017). N and S can be decomposed along parallel and perpendicular cutting directions to obtain the cutting force F_c and normal force F_n. Because the rake face of conventional PDC cutters is flat, the force analysis is relatively easy. For the Stinger PDC cutter, there is still existence squeezing force N and fraction force S like the conventional PDC cutter. But the direction of N and S is changed with the place of force application on the three-dimensional conical surface, which makes the derivation of cutting force and normal force becomes complex and difficult (Xiong et al., 2021). Thus, in this part, we want to obtain a phenomenological cutting force model for Stinger PDC cutters based on the above experimental data.

Numerous phenomenological cutting force models of conventional PDC cutters are based on the assumption that the cutting force is proportional to the cross-section area. Is there a similar quantity relationship between the cutting force and the cross-section area for Stinger PDC cutters? As shown in Figs. 10(a-2) and (a-3), the real contact area between the cutter and the rock, namely the interaction area S_1, is an arc plane. The cross-section area S_2 of cutting grooves is an elliptic arc plane. They are the function of cutting depth h and cutting angle α. The cross-section area S_2 is a projection area of the interaction area S_1 along a plane perpendicular to the cutting direction. For the Stinger PDC cutter, in the cutting process, the real contact area between the cutter and rock is a three-dimensional conical surface *G-DAC* as shown in Figs. 10(b-2). The cross-section area, in theory, is an isosceles triangle as shown in Figs. 10(b-3). But actually, the shape of the cross-section area of the cutting groove is irregular as shown in Fig. 5, and it is difficult to assess the cross-sectional area quantitatively. The three-dimensional squeezing force on the interaction area has the action to make the micro-cracks propagate to the sides of the cutting direction, which causes the cross-section of the cutting groove to be irregular. On the other hand, the interaction area is the real contact surface between the Stinger PDC cutter and rock, and the squeezing force and friction force are acted on this area. Exploring the relationship between the interaction area and the cutting force may be more reasonable for the Stinger PDC cutter.

Figs. 10(b-2) shows the schematic of the interaction area between Stinger PDC cutters and rock. The interaction area S_{r-c} is the three-dimensional conical surface *G-DAC*. S_{r-c} can be derived and expressed as Eq. (4). The detailed derivation process is shown in Appendix A.

$$S_{r-c}=\sqrt{2}a^2\int_0^{\frac{\pi}{2}}\sqrt{K_1\cos^4\beta+K_2\cos^3\beta+K_3\cos^2\beta+K_4\cos\beta+K_5}\cdot d\beta \tag{4}$$

where $K_1=-2A^2$, $K_2=-2AB$, $K_3=-2A^2-A$, $K_4=-B$, and $K_5=1-A$. In addition, $A=\sin^2\alpha$ and $B=m/a$, m and a are denoted as:

$$\begin{aligned} a&=h\cdot\frac{1+\tan^2\alpha}{1-\tan^2\alpha}\\ m&=a-h\frac{1-\tan\alpha}{1+\tan\alpha}\end{aligned} \tag{5}$$

where α is the cutting angle; h is the cutting depth.

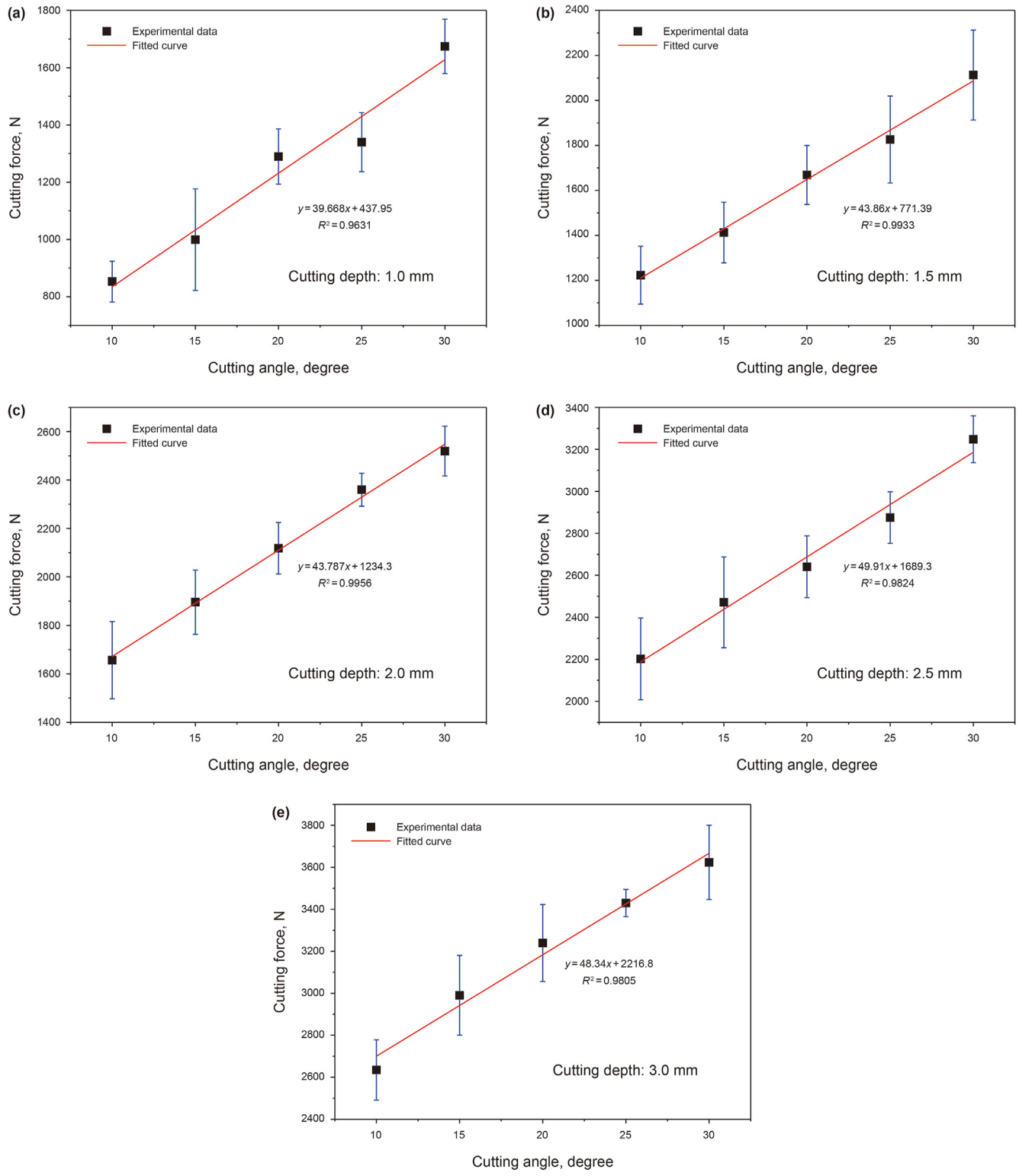

Fig. 8. The variation of cutting force with cutting angle at different cutting depths.

It can be found that the integrand in Eq. (4) is a function without an elementary antiderivative. Hence, in this paper, we use the fundamental theorem of calculus to compute the integral Eq. (4) by programming. The calculating results are shown in Fig. 11. The interaction area significantly increases with the increase of cutting depths for a constant cutting angle as shown in Fig. 11(a). But the larger the cutting angle, the more obvious the interaction area changes with the cutting depth. Fig. 11(b) shows the variation of interaction area with cutting angles at different cutting depths. With the increase of cutting angles, the interaction area gradually increases. It can be noted that when the cutting angle is smaller than 20°, the interaction area slightly increases with the rise of

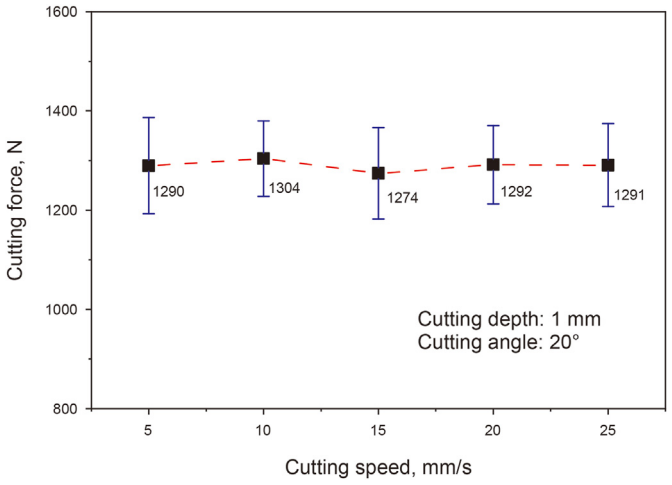

Fig. 9. The variation of cutting force with cutting speed.

cutting angles. When the cutting depth is 1 mm, the changes in cutting angle nearly have no e on the interaction area. By comparing Fig. 11(a) and (b), it can be concluded that cutting depths have a great influence on the interaction area than cutting angles. Combined with the experimental results in Section 3.1, we can reasonably guess that there is a certain correspondence between the interaction area and the cutting force.

Setting the interaction area as x-axis and cutting force as y-axis, the variation of cutting force with the interaction area is plotted in Fig. 12. By nonlinear fitting analysis, it is found that there is a quadratic polynomial correlation between the cutting force and the interaction area. The cutting force can be expressed as:

$$F_c = -1.63S^2 + 135.86S + 815.75 \quad R^2 = 0.9670 \tag{6}$$

where F_c is the cutting force, N; S is the interaction area, mm^2. The cutting force increases obviously when the interaction area increases, however, the increasing rate reduces with a larger interaction area. When the interaction area is equal to 0, the cutting force is 815.75 N, which represents the friction force acting on the spherical part of the Stinger PDC cutter's tip. This friction force is mainly affected by the rock properties and diameter of the cone tip. Although this model is obtained by regression from the experimental data, it still can be used to establish the force response model of hybrid PDC bits and optimize the bit design.

3.3. Influence of cutting parameters on MSE

MSE is a good index for evaluating rock-breaking efficiency. Fig. 13(a) shows the tendency of MSE with the increase in cutting depth. In general, the MSE versus cutting depth under different cutting angles present a similar tendency, i.e., as the cutting depth increases, MSE can be remarkably reduced. This is because the rock failure mode transforms from ductile mode to brittle model when the cutting depth gradually increases (Dai et al., 2020; He and Xu, 2016; Zhou and Lin, 2013). When the cutting depth is shallow, the rock contacted with the Stinger PDC cutter is mainly compressed into powder-like cuttings and the rock failure is dominated by ductile mode. As the cutting depth is deep, although there is still

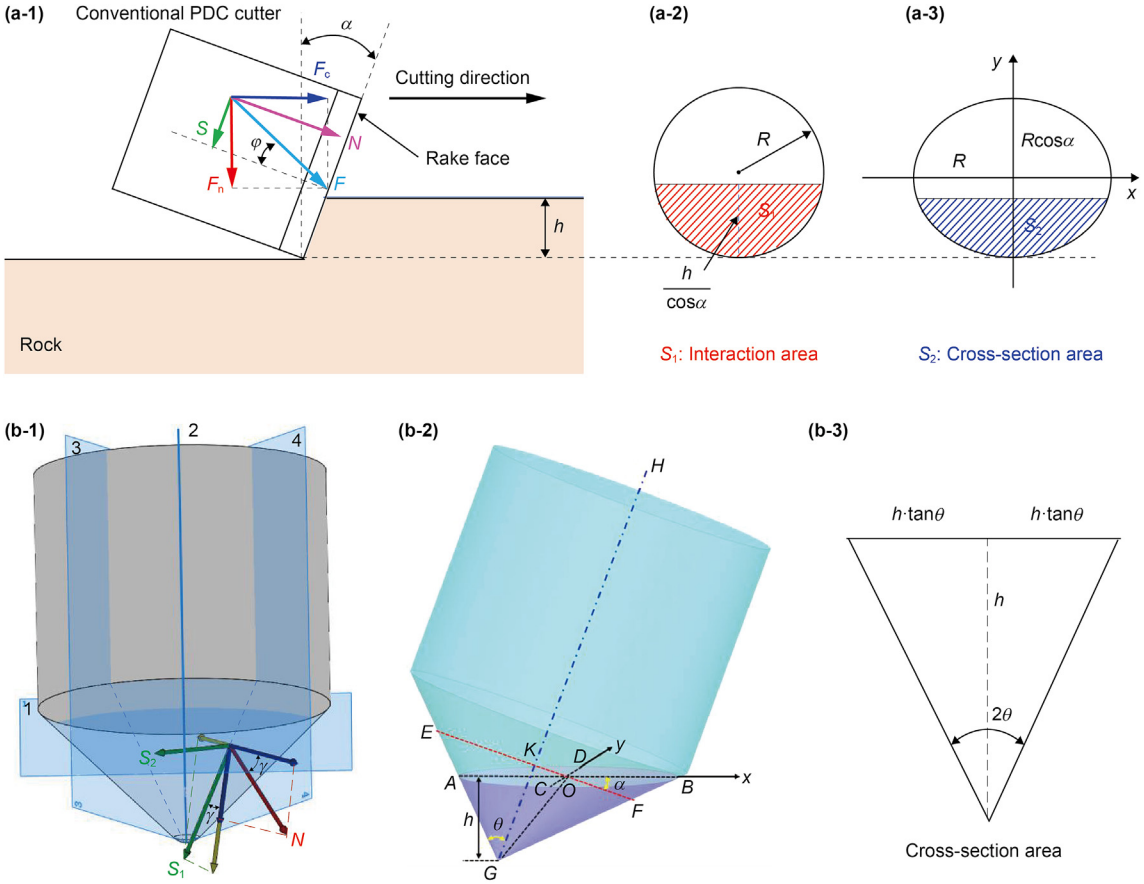

Fig. 10. Schematic of force responses, interaction area, and cross-section area of two cutters.

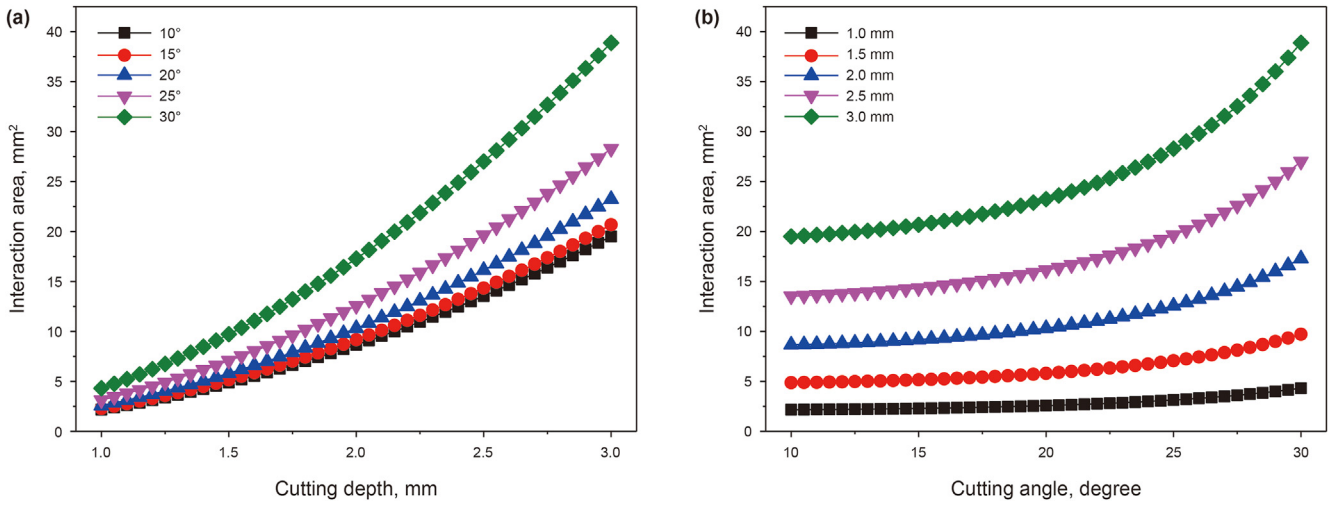

Fig. 11. The variation of interaction area with cutting depth and cutting angle.

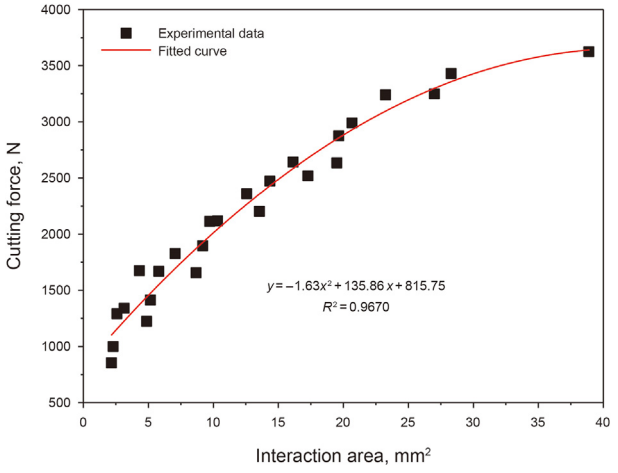

Fig. 12. The variation of cutting force with the interaction area.

existence of ductile failure mode around Stinger PDC cutters tip, the micro-cracks initiate at the periphery of the crushing area and propagate to rock-free surface to generate large size debris (Xiong et al., 2020b). This failure process is mainly dominated by the brittle mode. With the increase in cutting depth, the proportion of brittle failure increases gradually. According to the new surface theory of Von Rittinger (Grady and Kipp, 1985), there is more energy needed to break the rock into smaller fragments. In addition, Cheng et al. (2018) also, through the single cutting tests for the conventional PDC cutter, concluded that the mass fraction of cuttings and MSE are related, and the higher the powderlike cuttings mass fraction is, the larger the MSE. Hence, the larger proportion of brittle failure in rock breaking usually means a lower MSE and higher rock-breaking efficiency. Therefore, MSE significantly reduced with increasing the cutting depth as shown in Fig. 13(a).

After each experiment, the cuttings are collected and sieved with different mesh size screens: 8 mesh (2.36 mm), 14 mesh (1.40 mm), 30 mesh (0.60 mm), and 60 mesh (0.30 mm). The cuttings from each group were weighed and the mass fraction of each group is calculated. The mass fraction is defined as the mass ratio of cuttings within a certain size range to all cuttings. Fig. 14 presents the variation of mass fraction of different size cuttings with the cutting depth at 20° cutting angle. Cuttings in the group of 60/+∞ mesh are very small and like powder, that is generated when the rock failure with the ductile mode. While the group of 0/8 mesh is the large size debris, which is produced by the brittle failure of rock. As the cutting depth increases from 1.0 to 3.0 mm, the mass fraction of powder-like cuttings, that is cuttings in the size group of 60/+∞ mesh, reduces significantly. It means that the rock breaking efficiency is improved and the MSE is reduced. This is consistent with the tendency of MSE versus cutting depth shown in Fig. 13(a).

By nonlinear fitting analysis, it can be found that there is a quadratic polynomial correlation between MSE and cutting depths. For the deeper cutting depth, the reducing rate of MSE gradually decreases. It is also reflected in the changes of cuttings mass fraction with the cutting depth. Fig. 14 shows that when the cutting depth reaches 2.5 mm, the mass fraction of powder-like cuttings and large size debris changes little with further increasing cutting depths. This indicates that when the cutting depth reaches a critical value, the proportion of brittle failure in rock will be kept constant, and the MSE will reduce slightly. In this paper, the critical depth is between 2.0 and 2.5 mm.

Fig. 13(b) shows the tendency of MSE with cutting angles under different cutting depths. With the increase of cutting angle, the MSE decreases first and then increases. When the cutting angle is nearly 20°, the MSE reaches the minimum value, which means the highest rock breaking efficiency. It can be attributed to the special rock breaking mechanism mode, that is plowing action, and the conical geometry shape of Stinger PDC cutters. On the one hand, increasing the cutting angle can promote the micro-cracks to propagate to the rock surface and enhance the effects of the plowing action, which can contribute to the generation of large size debris, and improve the rock-breaking efficiency and reduce the MSE (Xiong et al., 2020b). On the other hand, increasing the cutting angle will significantly increase the interaction area. As shown in Fig. 11(b), the interaction area increases with cutting angles, especially when the cutting angle is larger than 20°, the increasing tendency is more obvious. The increase of interaction area will enlarge the magnitude of the normal squeezing force and sharply increase the friction force. A lot of energy will be dissipated as heat and can't help to break rock (Akbari et al., 2014; Che et al., 2017; Rafatian et al., 2010; Rostamsowlat et al., 2018). Thus, the MSE will increase. When the cutting angle is larger than 20°, the increase of friction force is the main factor affecting the MSE. As a result, the MSE increases as the cutting angle is larger than 20° shown in Fig. 13(b). During the design of the hybrid PDC bit, the Stinger PDC

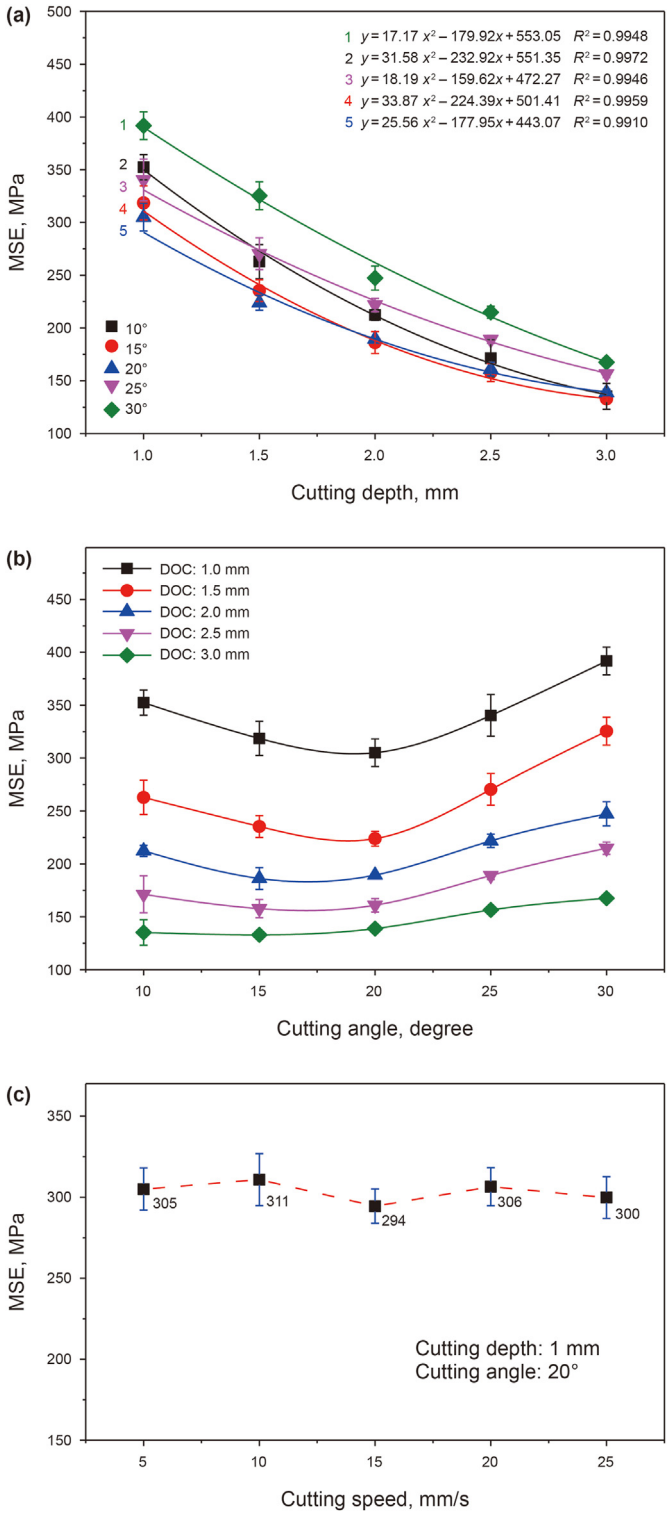

Fig. 13. The variation of MSE with the cutting depth, the cutting angle, and the cutting speed.

cutters are preferentially arranged with 20° former rake angle.

Fig. 13(c) shows the variation of MSE with cutting speed. It is clearly shown that the cutting speed has nearly no effect on the MSE. Many researchers also obtained a similar conclusion for the conventional PDC cutter, especially at the low cutting speed. Che et al. (2017) and Liu and Zhu (2019) believed that the cutting

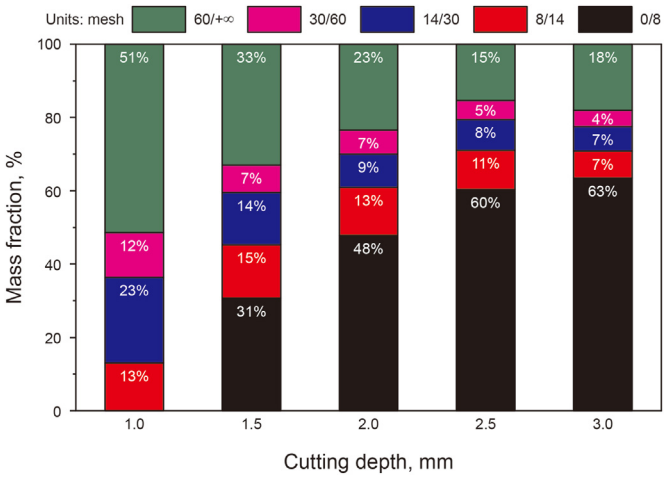

Fig. 14. The variation of cuttings mass fraction with the cutting depth for 20° cutting angle.

speed has little influence on the chip formation and the size and number of generated chips. It indicates that the cutting speed has little influence on the MSE. Majidi et al. (2011) found that MSE stays constant till about 100 RPM above which MSE slightly decreases with an increase in RPM. It is because a larger cutting speed helps to clear the fragmented cuttings from in front of the cutter and improves the rock breaking efficiency. Cheng et al. (2018) also conclude that MSE slightly reduces with increasing cutting speeds by experiment. In this paper, the cutting speed is relatively small. Therefore, the cutting speed nearly does not influence MSE.

3.4. Experimental repeatability and reproducibility

To evaluate the reliability of experimental results, experimental repeatability and reproducibility analyses were conducted. In this paper, the coefficient of variation (CV) (Hong et al., 2021; Pryseley et al., 2010) was used to calculate the repeatability of the measurement values, which can be expressed as:

$$CV = \frac{\sigma}{\mu} \times 100\% \tag{7}$$

where σ represents standard deviation; μ is the average value. Table 3 shows the coefficient of variations for the experimental results. The maximum value of CV for cutting force, rock broken volume, and MSE is 17.73%, 13.79%, and 10.27%, respectively. They are smaller than 20%, which indicates the experimental results have adequate repeatability.

4. Discussion

4.1. Surface topography and fracture morphology analysis

The cutting groove and large size debris are produced when the rock is broken by Stinger PDC cutters. The failure surface of these rock fragmentation products retains intuitive and primeval evidence for revealing rock breaking mechanisms (Che et al., 2016; Cheng et al., 2019b; Zeuch et al., 1983; Zuo et al., 2007). In this section, surface topography and fracture morphology of a cutting groove and large-size cuttings were measured by a 3D profilometer and a scanning electron microscope (SEM). Fig. 15 clearly presents the surface topography of a cutting groove and large-size cuttings, which were generated in the cutting tests with 2 mm cutting depth and 20° cutting angle. As shown in Fig. 15(a), the edge of cutting

grooves is very irregular, showing a serrated shape. The maximum width of the cutting groove is 24.23 mm, and the minimum width is 5.45 mm. The formation of irregular cutting groove edges can be attributed to the fact that the micro-cracks propagate to two sides of the cutting direction and generate large-size cuttings (Xiong et al. 2020a, 2020b). Furthermore, there is a narrow groove (blue area) with a width of about 2 mm at the center of cutting grooves. This is because the rock in the tip area of Stinger PDC cutters is compressed into powder-like cuttings due to the high point load (German et al., 2015; Radhakrishnan et al., 2016). The width of the compression area is equal to the cone tip diameter of Stinger PDC cutters as shown in Fig. 3(a).

The largest size debris was produced at location A in Fig. 15(a). The surface topography of the upper surface and lower surface were presented in Fig. 15(b) and (c). It should be noted that the failure surface in the upper surface was produced when large size cuttings was formed last time, while the failure surface in the lower surface was generated when large size cuttings was formed this time. The points on the failure surface along with line OB and line OC were extracted and the shape of the failure surface was shown in Fig. 15(d) and (f). It can be seen clearly that the shape of the fracture surface is arc-shaped. The parameter Sa (arithmetical mean deviation of the surface) was usually used to evaluate the surface roughness, which can reflect the rock failure mode. When the rock is broken by tensile stress, the surface is relatively rough, while the asperities on the rock surfaces will be crushed during the shearing action and the surface roughness will reduce (Sun and Li, 2019). The surface roughness of the side-wall (area I) and the bottom area (area II) of the cutting groove and the fracture surface in the upper and lower surface of large-size cuttings were measured and shown in Fig. 15(e). It is clearly presented that the surface roughness of the side-wall (area I) is significantly larger than the bottom area (area II). In addition, the surface roughness of the lower fracture surface and upper fracture and the side-wall (area I) are very close. This indicates that the rock failure mode at the bottom is significantly different from the side-wall and the mechanism of the formation of large-size debris is the same every time.

To further reveal which kind of force is dominating in rock breaking, the fracture morphology of cutting grooves and large size cuttings was observed and the SEM images are shown in Fig. 16. It can be seen that there are many micro-cracks and fine powder particles at the bottom area (area II) shown in Fig. 16(a) and (b). This is because the high point load applied by Stinger PDC cutters not only compresses the rock into fine powder cuttings but also induces micro-cracks at the bottom area of cutting grooves. Fig. 16(c), (d), (e), and (f) shows the fracture morphology of side-wall (area I) of cutting grooves and the lower fracture surface of large-size cuttings. These fractures mainly appear transgranular type, which possesses characteristics of river-like patterns, cleavage steps, lacerated ridges, and triangular pits. They are the typical characteristics of tensile fracture (Xiong et al., 2020b; Xu et al., 2008; Zuo et al., 2007). Thus, combined with the measurement results of the surface roughness mentioned above, it can be concluded that the micro-cracks propagating to two sides of the cutting direction and forming the large size cuttings is controlled by tensile stress. Moreover, it is general knowledge that the compressive strength and shear strength of rock is larger than its tensile strength. Rock is easy to break under tension. Hence, the Stinger PDC cutter breaks rock mainly with tensile stress, which is one of the most important reasons for the high rock breaking efficiency.

4.2. Rock breaking mechanism of stinger PDC cutters

Based on the above experimental analysis and our previous works (Xiong et al. 2020a, 2020b, 2022), the rock-breaking mechanism of Stinger PDC cutters can be revealed as shown in Fig. 17. Due to the innovative conical shape, the Stinger PDC cutter can

Table 3
Repeatability of experimental results.

No.	Cutting speed, mm/s	Cutting angle, degree	Depth of cut, mm	Cutting force, N			Rock broken volume, mm^3			MSE, MPa		
				Mean	SD	CV, %	Mean	SD	CV, %	Mean	SD	CV, %
1	5	10	1.0	853.00	71.30	8.36	241.83	12.38	5.12	352.37	11.94	3.39
2			1.5	1222.93	128.79	10.53	465.00	37.58	8.08	262.87	16.13	6.14
3			2.0	1656.77	159.13	9.60	781.40	86.56	11.08	212.27	5.19	2.45
4			2.5	2202.07	194.99	8.85	1318.43	47.87	3.63	171.23	17.59	10.27
5			3.0	2634.97	143.42	5.44	1953.87	89.85	4.60	135.17	12.14	8.98
6	5	15	1.0	999.47	177.16	17.73	312.50	39.57	12.66	318.53	16.09	5.05
7			1.5	1412.73	134.87	9.55	602.70	83.13	13.79	235.33	10.36	4.40
8			2.0	1895.97	132.67	7.00	1018.30	39.71	3.90	186.13	10.41	5.59
9			2.5	2471.40	216.31	8.75	1565.47	61.77	3.95	157.70	8.51	5.40
10			3.0	2990.17	190.207	6.36	2249.40	106.15	4.72	132.87	2.21	1.66
11	5	20	1.0	1289.67	96.80	7.51	422.77	23.06	5.45	305.00	13.04	4.28
12			1.5	1668.50	131.30	7.87	747.03	80.61	10.79	223.80	7.00	3.13
13			2.0	2118.03	106.20	5.01	1117.70	51.63	4.62	189.47	0.85	0.45
14			2.5	2640.53	147.28	5.58	1640.67	30.18	1.84	160.87	6.34	3.94
15			3.0	3239.43	183.03	5.65	2333.47	93.00	3.99	138.77	3.03	2.18
16	5	25	1.0	1339.93	103.15	7.70	395.10	43.59	11.03	340.30	19.70	5.79
17			1.5	1826.13	193.13	10.58	674.40	44.15	6.55	270.40	14.97	5.54
18			2.0	2360.00	68.12	2.89	1065.30	59.80	5.61	221.77	6.36	2.87
19			2.5	2874.70	122.82	4.27	1522.03	94.99	6.24	189.00	3.77	2.00
20			3.0	3429.93	64.89	1.89	2194.23	88.22	4.02	156.40	3.50	2.24
21	5	30	1.0	1674.47	94.62	5.65	427.53	22.62	5.29	391.77	13.15	3.36
22			1.5	2112.77	199.81	9.46	648.57	37.96	5.85	325.33	13.14	4.04
23			2.0	2519.43	102.75	4.08	1020.63	73.86	7.24	247.30	11.43	4.62
24			2.5	3248.03	111.59	3.44	1513.30	93.64	6.19	214.87	5.77	2.69
25			3.0	3623.57	176.47	4.87	2164.50	115.91	5.35	167.43	2.90	1.73
26	10	20	1.0	1303.97	76.02	5.83	419.53	13.06	3.11	310.87	16.00	5.15
27	15			1274.23	91.92	7.21	432.37	15.50	3.59	294.50	10.61	3.60
28	20			1291.53	78.80	6.10	421.23	13.76	3.27	306.53	11.75	3.83
29	25			1290.83	83.41	6.46	430.40	16.03	3.72	299.80	12.87	4.29

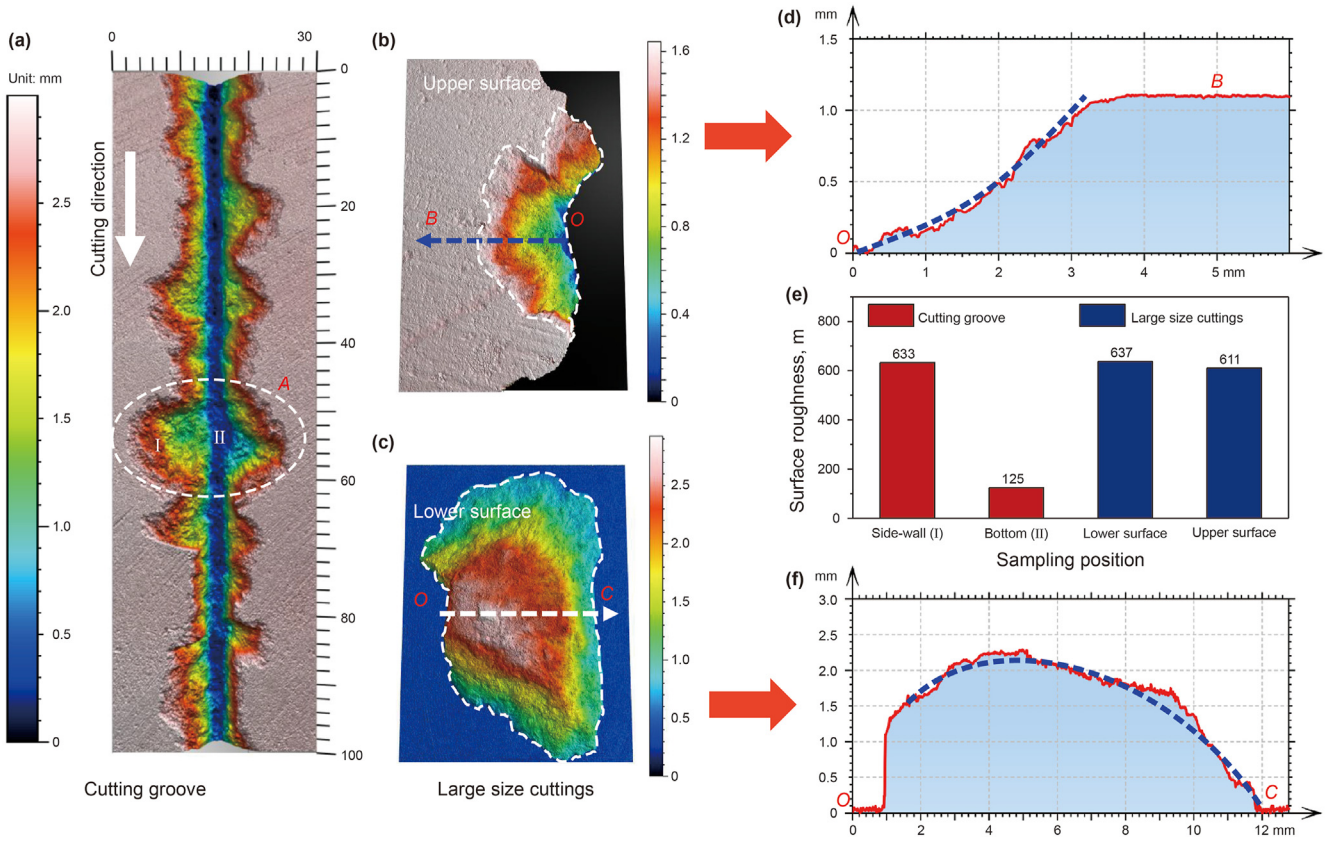

Fig. 15. Surface topography of a cutting groove and large size cuttings.

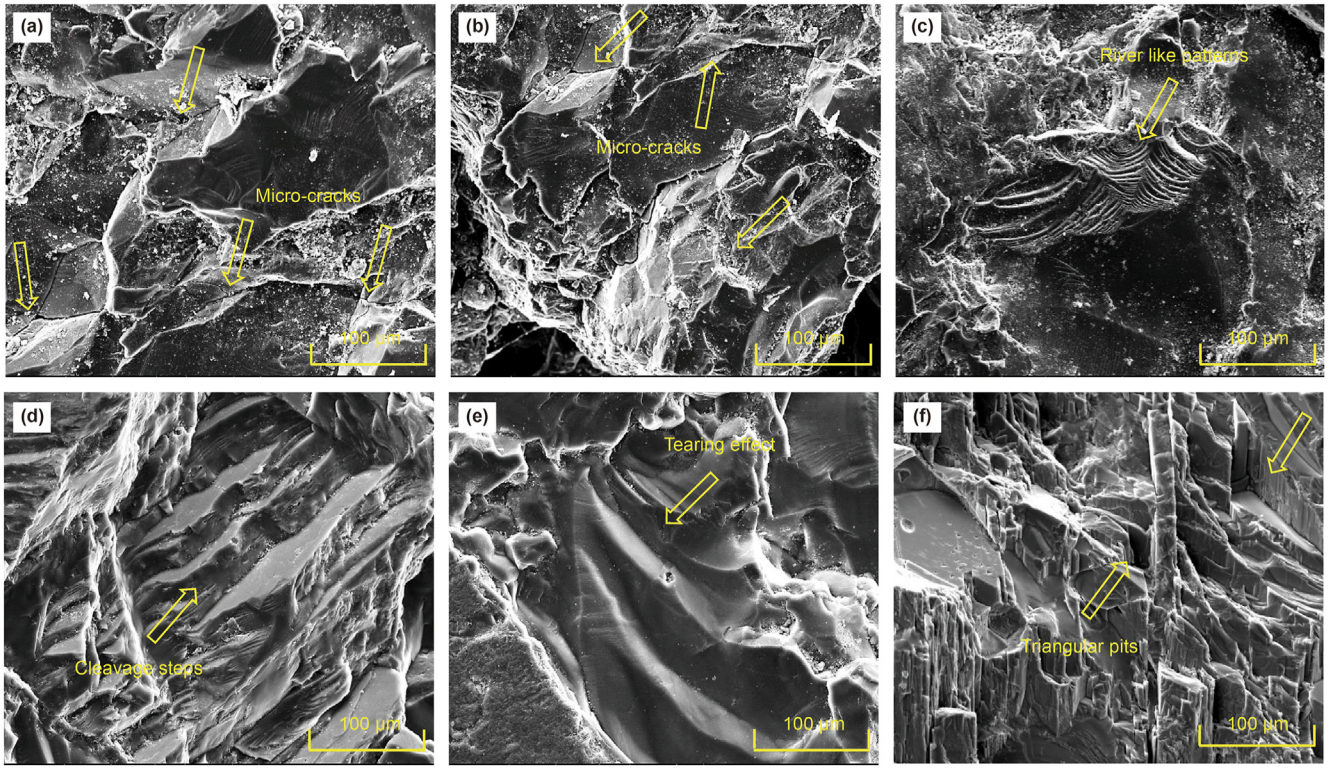

Fig. 16. The fracture morphology of the cutting groove and large size cuttings.

create a concentrated point loading at the cutter tip (German et al., 2015; Radhakrishnan et al., 2016), which compresses the rock and forms a crushed zone (Cheng et al., 2018; Zeuch et al., 1983). In this zone, the rock is squeezed into powder-like cuttings. After the cutting tests, the powder-like cuttings are cleaned and the obtained real cutting depth is larger than the set cutting depth. It clearly shows that the real cutting depth is nearly 3 mm in Fig. 15(a), while the set cutting depth is 2 mm. Furthermore, there are numerous micro-cracks initiated at the periphery of the crushed zone (Souissi et al., 2015). As the cutter moves forward, the micro-cracks induced at the front of cutters propagate to the rock surface and form the main crack under the tensile stress (Cheng et al., 2019a; Xiong et al., 2020b). The main crack is arc-shaped, which has been proved in Section 4.1 by surface topography analysis. Then, the volumetric breakage occurs and the large size cuttings are produced. In addition, due to the micro-cracks, the damaged area at the bottom of cutting grooves is formed and these micro-cracks have been clearly observed in Fig. 16(a) and (b). The formation of the damaged area can help to improve the rock breaking efficiency of the next cutting, which has been proved by the experiment in our previous works (Xiong et al., 2022). The rock-breaking mechanism can be summarized as: the high concentrated point loading is easy to induce the micro-cracks in the rock; the tensile stress significantly promotes the propagation of micro-cracks and produce the large size debris. Thus, under the double effects of the high concentrated point loading and tensile failure, the Stinger PDC cutter can achieve the high rock-breaking efficiency.

So according to our rock breaking mechanism model of Stinger PDC cutters, the periodical oscillations of cutting force shown in Fig. 4 can be explained and the reasonability of our model can be further proven. When $T = t$, the cutter finishes a cutting period and begins a new cutting period. Due to the large size cuttings flying out from the rock surface, the most of rock in front of the cutter has been removed. The cutting force decreases to the minimum value. As the cutter further moves forward and compresses the rock, the cutting force gradually increases. In this phase, the rocks directly contacted with the cutter are crushed into the fine powder and the cutting force fluctuates slightly. When $T = t + t_0$, the micro-crack propagates to the rock surface and form the main crack. The large size debris is formed and the cutting force reaches a peak. Due to the strain energy release, the debris flies out from the rock surface. The contact relation in the cutting direction between the cutter and rock is broken. The cutting force is rapidly dropped. This cutting period ends and begins the next cutting period. The rock breaking repeats the above process and the cutting force also repeats a process: gradually increasing, reaching a peak, and then decreasing rapidly.

5. Conclusions

In this paper, a series of single cutter tests were carried out with a Stinger PDC cutter, and the influences of cutting depth, cutting angle, and cutting speed on cutting force and MSE were analyzed. The mechanism of Stinger PDC cutters breaking hard rock was revealed. The major conclusions can be obtained as follows:

(1) The cutting force increases linearly with the increase of cutting depth and cutting angle. Cutting speed has no obvious effect on the cutting force, and cutting depth has the largest influence.
(2) The interaction area between the Stinger PDC cutter and rock increases with increasing cutting depth and cutting angle. Cutting depth has a great influence on the interaction area than cutting angles. There is a good quadratic polynomial relationship between the cutting force and the interaction area.
(3) The MSE remarkably decreases with increasing cutting depth. The cutting speed has few influence on the MSE. With the increase of cutting angle, MSE gradually decreases first and then increases. When the cutting angle is nearly 20°, MSE reaches minimum values, which means the highest rock-breaking efficiency. In the design of cutter arrangement for hybrid PDC bits, the inclination angle of Stinger PDC cutters is preferably 20°.
(4) The Stinger PDC cutter breaking rock mainly depends on the high concentrated point loading and the tensile failure, which can significantly improve the rock-breaking efficiency.

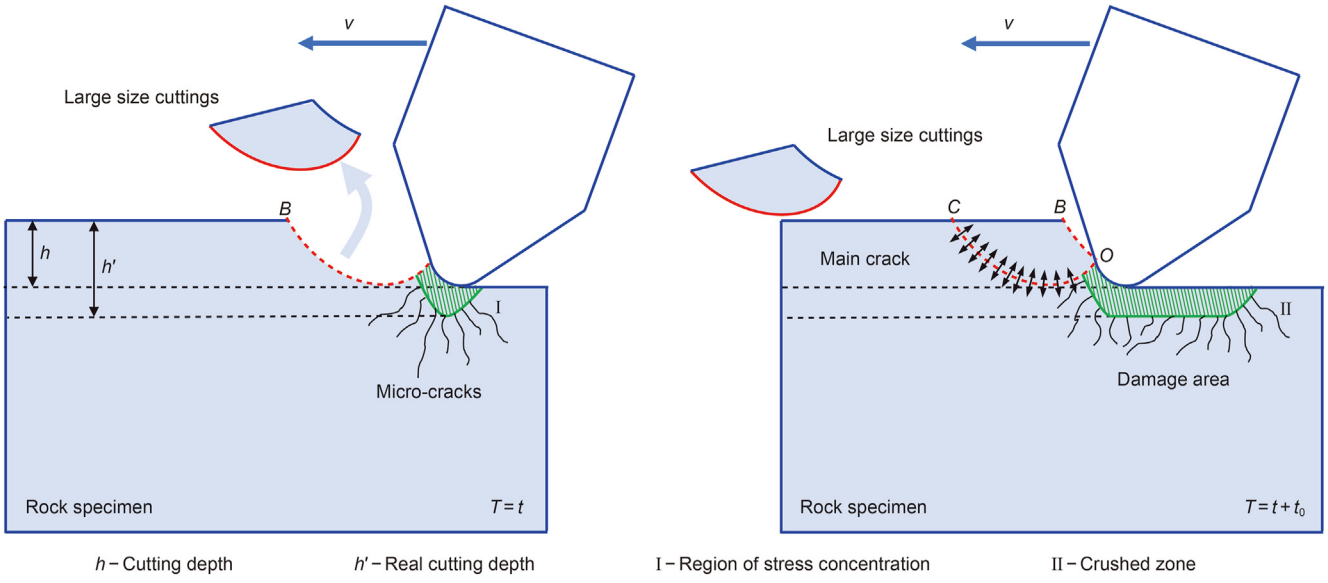

Fig. 17. The schematic of the rock breaking mechanism of the Stinger PDC cutter.

Acknowledgments

This work has been supported by the Joint Funds of The National Natural Science Foundation of China (Grant No. U19B6003-05), the National Key Research and Development Program of China (No. 2019YFA0708302), the National Science Fund for Distinguished Young Scholars (Grant No. 51725404), the Beijing Outstanding Young Scientist Program (Grant No. BJJWZYJH01201911414038), and the Strategic Cooperation Technology Projects of CNPC and CUPB (Grant No. ZLZX2020-01).

Appendix A. Derivation of interaction area between Stinger PDC cutter and rock

In this section, the detailed derivation process of Eq. (4) is provided. Fig. A-1(a) shows the schematic of the interaction area. The cone tip diameter of the Stinger PDC cutter is ignored in this derivation due to its little influence on the interaction area. The interaction area between the Stinger PDC cutter and the rock is the three-dimensional conical surface *G-DAC*. The plane *xoy* coincides with the top surface of the rock, which is the horizontal plane. The intersection line of the Stinger PDC cutter and the horizontal plane is an ellipse. It can be expressed by:

$$\frac{x^2}{a^2}+\frac{y^2}{b^2}=1 \quad (a>b>0) \tag{A-1}$$

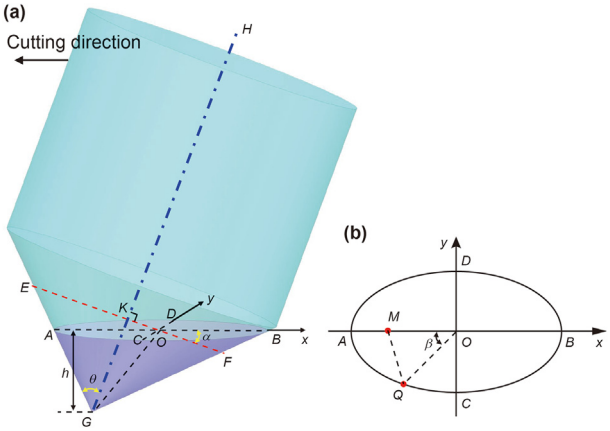

Fig. A-1. Schematic of the interaction area between the Stinger PDC cutter and the rock

Thus, $\overline{OA}=\overline{OB}=a$, $\overline{OD}=\overline{OC}=b$. In addition, the cone tip angle $\angle AGB$ is $\pi/2$ as shown in Fig. 3(a). Hence, $\overline{OG}=\overline{OA}=\overline{OB}=a$. The points *E*, *C*, *F*, *D* are located on a circle, which is perpendicular to the axis of the Stinger PDC cutter *GH*, and the center of the circle is point *K*. Thus, $\overline{KE}=\overline{KC}=\overline{KF}=\overline{KD}$. The angle between this circle and the horizontal plane is the cutting angle α. According to the geometrical relationships, the following equations can be obtained: $\angle KFG=\pi/4$, $\angle OBG=\angle OGB=\pi/4-\alpha$, $\angle KOG=\angle KFG+\angle OGB=\pi/4+\pi/4-\alpha=\pi/2-\alpha$. In Rt$\Delta OKG$, $\overline{KG}=\overline{OG}\cdot\sin(\angle KOG)=a\cdot\cos\alpha$, $\overline{KO}=\overline{OG}\cdot\cos(\angle KOG)=a\cdot\sin\alpha$. In Rt$\Delta KOD$, there is the following relationship:

$$b=\overline{OD}=\sqrt{\overline{KD}^2-\overline{KO}^2}=\sqrt{(a\cdot\cos\alpha)^2-(a\cdot\sin\alpha)^2}$$
$$=a\sqrt{\cos^2\alpha-\sin^2\alpha} \tag{A-2}$$

In RtΔAGB, $\angle GAB=\pi/2-\angle OBG=\pi/4+\alpha$. Therefore, $\overline{AB}$ can be expressed as:

$$\overline{AB}=\frac{h}{\tan(\angle GAB)}+\frac{h}{\tan(\angle GBA)}=2h\cdot\frac{1+\tan^2\alpha}{1-\tan^2\alpha}=2a \tag{A-3}$$

where h is the cutting depth.

Point *M* is the projection of the vertex *G* of the Stinger PDC cutter into the horizontal plane as shown in Fig. A-1(b). The line from any point $Q(-a\cdot\cos\beta,-b\cdot\sin\beta)$ on the elliptic arc *AC* to point *G* is the hypotenuse of a right triangle, and the other two legs of the right triangle are $\overline{MQ}$ and the cutting depth h, respectively. Hence, set $m=\overline{OM}$, it can be expressed as:

$$m=\overline{OA}-\overline{MA}=a-\frac{h}{\tan(\angle GAB)}=a-h\frac{1-\tan\alpha}{1+\tan\alpha} \tag{A-4}$$

The point *M* is $(-m,0)$ and the point *Q* is $(-a\cdot\cos\beta,-b\cdot\sin\beta)$. Therefore, the length of the line segment $\overline{GQ}$ can be expressed as:

$$\overline{GQ}=\sqrt{\overline{MQ}^2+h^2}$$
$$=\sqrt{a^2\cos^2\beta+b^2\sin^2\beta+m^2-2am\cos\beta+h^2} \tag{A-5}$$

When $\beta=\pi/2$, $\overline{GQ}=\overline{GC}$, and $\overline{GC}=\overline{GE}=\sqrt{2}\overline{GK}=\sqrt{2}a\cos\alpha$. Thus, there is the following equation:

$$b^2+m^2+h^2=2a^2\cos^2\alpha \tag{A-6}$$

Substituting Eq. (A-2) into Eq. (A-6) gives:

$$\begin{aligned} &m^2+h^2=a^2\\ &a^2+b^2=2a^2\cos^2\alpha\\ &a^2-b^2=2a^2\sin^2\alpha \end{aligned} \tag{A-7}$$

Substitute Eq. (A-7) into Eq. (A-5), $\overline{GQ}$ can be simplified as:

$$\overline{GQ}=\sqrt{2a^2\sin^2\alpha\cos^2\beta-2am\cos\beta+2a^2\cos^2\alpha} \tag{A-8}$$

The interaction area S_{r-c} can be derived by integrating β, it can be expressed as:

$$S_{r-c}=2\int_0^{\frac{\pi}{2}}\frac{1}{2}\cdot\overline{GQ}\cdot\mathrm{d}s=\int_0^{\frac{\pi}{2}}\sqrt{2a^2\sin^2\alpha\cos^2\beta-2am\cos\beta+2a^2\cos^2\alpha}\cdot$$
$$\sqrt{a^2\sin^2\beta+b^2\cos^2\beta}\cdot\mathrm{d}\beta=\sqrt{2}a^2\int_0^{\frac{\pi}{2}}\sqrt{\sin^2\alpha\cos^2\beta-\frac{m}{a}\cos\beta+\cos^2\alpha}\cdot$$
$$\sqrt{1-2\sin^2\alpha\cos^2\beta}\cdot\mathrm{d}\beta \tag{A-9}$$

Set $A=\sin^2\alpha$, $B=m/a$, Eq. (A-9) can be expressed as:

$$S_{r-c} = \sqrt{2}a^2 \int_0^{\frac{\pi}{2}} \sqrt{-2A^2\cos^4\beta + 2AB\cos^3\beta + \left(2A^2 - A\right)\cos^2\beta - B\cos\beta + (1-A)} \cdot \mathrm{d}\beta \quad \text{(A-10)}$$

Set $K_1 = -2A^2$, $K_2 = 2AB, K_3 = 2A^2 - A, K_4 = -B, K_5 = 1 - A$, Eq. (A-10) can be expressed as:

$$S_{r-c} = \sqrt{2}a^2 \int_0^{\frac{\pi}{2}} \sqrt{K_1\cos^4\beta + K_2\cos^3\beta + K_3\cos^2\beta + K_4\cos\beta + K_5} \cdot \mathrm{d}\beta \quad \text{(A-11)}$$

References

Akbari, B., Miska, S., Yu, M., et al., 2014. The effects of size, chamfer geometry, and back rake angle on frictional response of PDC cutters. 48th US rock mechanics/geomechanics symposium. In: https://onepetro.org/ARMAUSRMS/proceedings/ARMA14/All-ARMA14/ARMA-2014-7458/123878.

Al-Enezi, D., Goswami, B., Takate, Y., et al., 2017. Conical diamond element on PDC bits sets new drilling performance benchmark in northern Kuwait field. SPE Middle East Oil & Gas Show and Conference. https://doi.org/10.2118/183781-MS.

Aresh, B., Khan, F.N., Haider, J., 2022. Experimental investigation and numerical simulation of chip formation mechanisms in cutting rock-like materials. J. Petrol. Sci. Eng. 209, 109869. https://doi.org/10.1016/j.petrol.2021.109869.

Azar, M., White, A., Velvaluri, S., et al., 2013. Middle east hard/abrasive formation challenge: reducing PDC cutter volume at bit center increases ROP/drilling efficiency. SPE/IADC Middle East Drilling Technology Conference & Exhibition. https://doi.org/10.2118/166755-MS.

Che, D., Ehmann, K., 2014. Experimental study of force responses in polycrystalline diamond face turning of rock. Int. J. Rock Mech. Min. Sci. 72, 80–91. https://doi.org/10.1016/j.ijrmms.2014.08.014.

Che, D., Zhang, W., Ehmann, K., 2017. Chip formation and force responses in linear rock cutting: an experimental study. J. Manuf. Sci. Eng. 139 (1), 011011. https://doi.org/10.1115/1.4033905.

Che, D., Zhang, W., Zhu, Z., et al., 2018. Rock fails in shearing as a tuned critical system. Int. J. Rock Mech. Min. Sci. 110, 133–139. https://doi.org/10.1016/j.ijrmms.2018.07.022.

Che, D., Zhu, W.-L., Ehmann, K.F., 2016. Chipping and crushing mechanisms in orthogonal rock cutting. Int. J. Mech. Sci. 119, 224–236. https://doi.org/10.1016/j.ijmecsci.2016.10.020.

Cheatham Jr., J., Daniels, W., 1979. A study of factors influencing the drillability of shales: single-cutter experiments with STRATAPAX (T) drill blanks. J. Energy Resour. Technol. 101 (3), 189–195. https://doi.org/10.1115/1.3446918.

Chen, P., Miska, S., Yu, M., et al., 2021. Modeling of cutting rock: from PDC cutter to PDC bit—modeling of PDC cutter. SPE J. 26 (6), 3444–3464. https://doi.org/10.2118/205342-PA.

Chen, S., Grosz, G., Anderle, S., et al., 2016. The role of rock-chip removals and cutting-area shapes in polycrystalline-diamond-compact-bit design optimization. SPE Drill. Complet. 30 (4), 334–347. https://doi.org/10.2118/171833-PA.

Cheng, Z., Li, G., Huang, Z., et al., 2019a. Analytical modelling of rock cutting force and failure surface in linear cutting test by single PDC cutter. J. Petrol. Sci. Eng. 177, 306–316. https://doi.org/10.1016/j.petrol.2018.09.023.

Cheng, Z., Sheng, M., Li, G., et al., 2019b. Cracks imaging in linear cutting tests with a PDC cutter: characteristics and development sequence of cracks in the rock. J. Petrol. Sci. Eng. 179, 1151–1158. https://doi.org/10.1016/j.petrol.2019.04.053.

Cheng, Z., Sheng, M., Li, G., et al., 2018. Imaging the formation process of cuttings: characteristics of cuttings and mechanical specific energy in single PDC cutter tests. J. Petrol. Sci. Eng. 171, 854–862. https://doi.org/10.1016/j.petrol.2018.07.083.

Coudyzer, C., Richard, T., 2005. Influence of the back and side rake angles in rock cutting. AADE 2005 National Technical Conference and Exhibition. https://www.aade.org/application/files/5415/7304/0403/AADE-05-NTCE-74_-_Coudyzer.pdf.

Dai, X., Huang, Z., Shi, H., et al., 2020. Rock failure analysis based on the cutting force in the single PDC cutter tests. J. Petrol. Sci. Eng. 194, 107339. https://doi.org/10.1016/j.petrol.2020.107339.

Dai, X., Huang, Z., Shi, H., et al., 2021a. Cutting force as an index to identify the ductile-brittle failure modes in rock cutting. Int. J. Rock Mech. Min. Sci. 146, 104834. https://doi.org/10.1016/j.ijrmms.2021.104834.

Dai, X., Huang, Z., Shi, H., et al., 2021b. A novel experimental apparatus for single polycrystalline diamond compact cutter tests. Rev. Sci. Instrum. 92 (1), 015109. https://doi.org/10.1063/5.0033425.

Dou, N., Yang, S., 2015. Simulation research of conical PDC cutter rock-breaking mechanism. Oil Field Equipment 44 (11), 12–17 (in Chinese). https://10.3969/j.issn.1001-3482.2015.11.003.

Durrand, C., Skeem, M., Hall, D., 2010. Thick PDC, shaped cutters for geothermal drilling: a fixed cutter solution for a roller cone drilling environment. 44th US Rock Mechanics Symposium and 5th US-Canada Rock Mechanics Symposium. In: https://onepetro.org/ARMAUSRMS/proceedings/ARMA10/All-ARMA10/ARMA-10-524/118075.

German, V., Pak, M., Azar, M., et al., 2015. Conical diamond element bit sets new performance benchmarks drilling extremely hard carbonate/chert formations, Perm region Russia. SPE/IADC Drilling Conference and Exhibition. https://doi.org/10.2118/173144-MS.

Glowka, D.A., 1989. Use of single-cutter data in the analysis of PDC bit designs: Part 1 - development of a PDC cutting force model. J. Petrol. Technol. 41 (8), 797–849. https://doi.org/10.2118/15619-PA.

Grady, D., Kipp, M., 1985. Geometric statistics and dynamic fragmentation. J. Appl. Phys. 58 (3), 1210–1222. https://doi.org/10.1063/1.336139.

Gunawan, F., Krisnanto, W., Mardiana, M., et al., 2018. Conical diamond element PDC bit as a breakthrough to drill hard geothermal formation in Indonesia. IADC/SPE Asia Pacific Drilling Technology Conference and Exhibition. https://doi.org/10.2118/191100-MS.

He, R., 2014. Numerical Simulation Study on Stinger PDC Cutter's Cutting Rock Process. Master Thesis. China University of Petroleum, (East China). https://kns.cnki.net/KCMS/detail/detail.aspx?dbname=CMFD201602&filename=1016711786.

He, X., Xu, C., 2015. Discrete element modelling of rock cutting: from ductile to brittle transition. Int. J. Numer. Anal. Methods GeoMech. 39 (12), 1331–1351. https://doi.org/10.1002/nag.2362.

He, X., Xu, C., 2016. Specific energy as an index to identify the critical failure mode transition depth in rock cutting. Rock Mech. Rock Eng. 49 (4), 1461–1478. https://doi.org/10.1007/s00603-015-0819-6.

Hempton, R., Copeland, C., Cox, G., et al., 2015. Innovative conical diamond element bits drill back-to-back tight curves in one run, improving economics while reducing risk in Avalon Shale Play. SPE Liquids-Rich Basins Conference-North America. Society of Petroleum Engineers, doi:10.2118/175534-MS.

Hong, C., Yang, R., Huang, Z., et al., 2021. Experimental investigation on coal-breakage performances by abrasive nitrogen-gas jet with a conical nozzle. Int. J. Rock Mech. Min. Sci. 142, 104781. https://doi.org/10.1016/j.ijrmms.2021.104781.

Jamali, S., Wittig, V., Börner, J., et al., 2019. Application of high powered laser technology to alter hard rock properties towards lower strength materials for more efficient drilling, mining, and Geothermal Energy production. Geomechanics for Energy and the Environment 20, 100112. https://doi.org/10.1016/j.gete.2019.01.001.

Jianyong, P., 2012. Interpretation of single cutter tests for rock mechanical properties. 46th US Rock Mechanics/Geomechanics Symposium. In: https://onepetro.org/ARMAUSRMS/proceedings/ARMA12/All-ARMA12/ARMA-2012-142/122211.

Liu, W., Zhu, X., 2019. Experimental study of the force response and chip formation in rock cutting. Arabian J. Geosci. 12 (15), 457. https://doi.org/10.1007/s12517-019-4585-8.

Liu, W., Zhu, X., Jing, J., 2018. The analysis of ductile-brittle failure mode transition in rock cutting. J. Petrol. Sci. Eng. 163, 311–319. https://doi.org/10.1016/j.petrol.2017.12.067.

Liu, Z., Hou, H., Hu, W., 2019. An experimental and numerical simulation study on rock cutting based on pre-breaking. China Petroleum Machinery 47 (12), 38–43+57 (in Chinese). https://10.16082/j.cnki.issn.1001-4578.2019.12.006.

Majidi, R., Miska, S.Z., Tammineni, S., 2011. PDC single cutter: the effects of depth of cut and RPM under simulated borehole conditions. Wiertnictwo, Nafta, Gaz. 28, 283–295. https://bibliotekanauki.pl/articles/299337.

Pryseley, A., Mintiens, K., Knapen, K., et al., 2010. Estimating precision, repeatability, and reproducibility from Gaussian and non-Gaussian data: a mixed models approach. J. Appl. Stat. 37 (10), 1729–1747. https://doi.org/10.1080/02664760903150706.

Radhakrishnan, V., Chuttani, A., Anggrani, F., et al., 2016. Conical diamond element technology delivers step change in directional drilling performance. IADC/SPE Asia Pacific Drilling Technology Conference. https://doi.org/10.2118/180515-MS.

Rafatian, N., Miska, S.Z., Ledgerwood, L.W., et al., 2010. Experimental study of MSE of a single PDC cutter interacting with rock under simulated pressurized conditions. SPE Drill. Complet. 25 (1), 10–18. https://doi.org/10.2118/119302-PA.

Rajabov, V., Miska, S.Z., Mortimer, L., et al., 2012. The effects of back rake and side rake angles on mechanical specific energy of single PDC cutters with selected rocks at varying depth of cuts and confining pressures. IADC/SPE Drilling

Conference and Exhibition. https://doi.org/10.2118/151406-MS.
Raymond, D.W., Knudsen, S.D., Blankenship, D.A., et al., 2012. PDC bits outperform conventional bit in geothermal drilling project. GRC Transactions 36, 307–316. https://www.osti.gov/biblio/1116394.
Richard, T., Coudyzer, C., Desmette, S., 2010. Influence of groove geometry and cutter inclination in rock cutting. 44th US rock mechanics symposium and 5th US-Canada rock mechanics symposium. In: https://onepetro.org/ARMAUSRMS/proceedings/ARMA10/All-ARMA10/ARMA-10-429/117992.
Rostamsowlat, I., Richard, T., Evans, B., 2018. An experimental study of the effect of back rake angle in rock cutting. Int. J. Rock Mech. Min. Sci. 107, 224–232. https://doi.org/10.1016/j.ijrmms.2018.04.046.
Schlumberger, 2022. StingBlade conical diamond element bit. https://www.slb.com/drilling/bottomhole-assemblies/drill-bits/blade-family-bits/stingblade-conical-diamond-element-bit.
Souissi, S., Hamdi, E., Sellami, H., 2015. Microstructure effect on hard rock damage and fracture during indentation process. Geotech. Geol. Eng. 33 (6), 1539–1550. https://doi.org/10.1007/s10706-015-9920-6.
Sun, D., Li, Q., 2019. Morphology variation analysis for rock surfaces before and after shearing. Geotech. Geol. Eng. 37 (2), 1029–1037. https://doi.org/10.1007/s10706-018-0670-0.
Sun, Y., Zou, D., Hou, X., et al., 2014. Test of force of conical PDC cutter during rock plow-breaking. China Petroleum Machinery 42 (9), 23–26. https://doi.org/10.3969/j.issn.1001-4578.2014.09.006 (in Chinese).
Teale, R., 1965. The concept of specific energy in rock drilling. Int. J. Rock Mech. Min. Sci. Geomech. Abstracts 2 (1), 57–73. https://doi.org/10.1016/0148-9062(65)90022-7.
Xiong, C., Dai, X., Shi, H., et al., 2020a. Investigation on rock breakage mechanism of Stinger PDC cutter and hybrid cutter arrangement design. 54th US Rock Mechanics/Geomechanics Symposium. In: https://onepetro.org/ARMAUSRMS/proceedings/ARMA20/All-ARMA20/ARMA-2020-1419/447548.
Xiong, C., Huang, Z., Shi, H., et al., 2022. Experimental investigation into mixed tool cutting of granite with Stinger PDC cutters and conventional PDC cutters. Rock Mech. Rock Eng. 55 (2), 813–835. https://doi.org/10.1007/s00603-021-02680-z.
Xiong, C., Huang, Z., Shi, H., et al., 2021. 3D cutting force model of a Stinger PDC cutter: considering confining pressure and the thermal stress. Rock Mech. Rock Eng. 54, 5001–5022. https://doi.org/10.1007/s00603-021-02494-z.
Xiong, C., Huang, Z., Yang, R., et al., 2020b. Comparative analysis cutting characteristics of stinger PDC cutter and conventional PDC cutter. J. Petrol. Sci. Eng. 189, 106792. https://doi.org/10.1016/j.petrol.2019.106792.
Xu, X.-L., Feng, G., Shen, X.-M., et al., 2008. Mechanical characteristics and microcosmic mechanisms of granite under temperature loads. J. China Univ. Min. Technol. 18 (3), 413–417. https://doi.org/10.1016/S1006-1266(08)60086-3.
Zeuch, D., Swenson, D., Finger, J., 1983. Subsurface damage development in rock during drag-bit cutting: observations and model predictions. The 24th US Symposium on Rock Mechanics (USRMS). In: https://onepetro.org/ARMAUSRMS/proceedings/ARMA83/All-ARMA83/ARMA-83-0733/129459.
Zhou, Y., Lin, J.-S., 2013. On the critical failure mode transition depth for rock cutting. Int. J. Rock Mech. Min. Sci. 62, 131–137. https://doi.org/10.1016/j.ijrmms.2013.05.004.
Zhu, X., Luo, Y., Liu, W., et al., 2022. Rock cutting mechanism of special-shaped PDC cutter in heterogeneous granite formation. J. Petrol. Sci. Eng. 210, 110020. https://doi.org/10.1016/j.petrol.2021.110020.
Zijsling, D., 1987. Single cutter testing - A key for PDC bit development. SPE Offshore Europe. Society of Petroleum Engineers, doi:10.2118/16529-MS.
Zuo, J.-P., Xie, H.-P., Zhou, H.-W., et al., 2007. Fractography of sandstone failure under temperature-tensile stress coupling effects. Chin. J. Rock Mech. Eng. 26 (12), 2444–2457. https://10.3321/j.issn:1000-6915.2007.12.009.